Electronic Supplementary Information

Experimental

Synthesis of CoY-MOF/NF

First, a piece of commercial Ni foam with an area of 2 × 4 cm^2 was washed with 3 M hydrochloric acid, ethanol and deionized water, then dried in a vacuum drying oven at 60 °C for use. 0.055 g of triethylenediamine (TED), 0.175 g of 1,4-benzenedicarboxylic acid (BDC), and 0.3 g $Co(NO_3)_2 \cdot 6H_2O$ were dispersed in 30 mL of N, N-dimethylformamide(DMF) by sonication and concomitant shaking to form a uniform and transparent pink solution. Subsequently, under vigorous stirring, aqueous YCl_3 solution (2 mL, 20 mM) was added dropwise to the above mixture and stirring was continued for 15 min. Then, the reaction solution and the pretreated Ni foam were added to a Teflon-lined autoclave (50 ml) and reacted in an oven (130 °C, 14 h). After the reaction, CoY-MOF/NF was obtained by washing several times with ethanol and then dried in an oven. The Co-MOF/NF counterpart was obtained by replacing the YCl3 solution with an equal amount of deionized water.

Characterizations

The morphology was characterized by scanning electron microscopy (SEM, Chase SUPRA 55), transmission electron microscopy (TEM, JEM-2010) and high-angle annular dark-field scanning electron microscopy (HAADF-STEM, JEM-2010). The samples were subjected to X-ray diffraction (XRD) using CuKα emission spectroscopy (λ = 0.154056 nm). X-ray photoelectron spectroscopy (XPS) measurements were carried out on an ESCALAB MK II spectrometer (VG Scientific, UK) using Al Kα X-rays as the light source. Fourier transform infrared (FT-IR) spectra were recorded using a PerkinElmer spectrometer (Spectrum II). Raman spectroscopic characterization was

performed on a LabRam HR UV800 laser micro Raman spectrometer (Jobin Yvon, France). Atomic proportions were calculated using inductively coupled plasma optical emission spectrometry (ICP-OES) (Thermo Fisher iCAP PRO). Nuclear magnetic resonance (NMR) (Avance III HD 500, Bruker) for quantitative and qualitative analysis of GOR products.

Electrochemical measurements

All electrochemical measurements were performed at room temperature using an electrochemical workstation (CHI 660E). Saturated Ag/AgCl was used as the reference electrode and graphite rod as the counter electrode. In addition, self-supporting CoY-MOF/NF (1 cm^2 geometric area) working electrode was used to evaluate HER and GOR performance. For comparison, RuO_2 and Pt/C loaded on Ni foam were also used as working electrodes with a loading of 1.0 mg. Electrolyte for HER measurement is 1.0 M KOH, and that for GOR is 1.0 M KOH with 0.1 M glycerol. Linear scanning voltammetry (LSV) was used to record the polarization curves of HER and GOR at a scan rate of 5 mV s^{-1}. The electrochemical impedance spectroscopy (EIS) of both HER and GOR were measured in the frequency range of 10^5 Hz to 10^{-1} Hz with an amplitude of 5 mV. Where the voltages were all converted to reversible hydrogen electrodes according to the Nernst equation with the equation: $E_{vs.RHE} = E^{\theta}_{Ag/AgCl} + E_{vs.Ag/AgCl} + 0.059*pH$. All polarization curves were corrected by iR compensation (95%), unless otherwise stated.

For constructing the HER-GOR co-electrolysis system, the CoY-MOF/NF was used as both cathode and anode, and electrocatalytic performance was evaluated under 1.0 M KOH with 0.1 M glycerol. The current density data were obtained by normalizing current to the geometric area of the working electrode unless otherwise stated.

As for HER-GOR co-electrolysis system, the H_2 production and formate production were evaluated by the drainage method and determined by ^1H NMR spectrometry (maleic acid as an internal standard), respectively. The corresponding calculation equations for Faradaic efficiency (FE) are as follows.[1, 2]

$$FE(H_2) = \frac{N(H_2\ production)}{Q_{tot1}/(Z_1 \times F)} \times 100\% \quad (1)$$

$$FE(formate) = \frac{N(formate\ yield)}{Q_{tot2}/(Z_2 \times F)} \times 100\% \quad (2)$$

Where Q_{tot1} is the total charge through the electrode during HER and Q_{tot2} is the total charge through the electrode during GOR. Z_1 is the number of electrons to produce one molecule of H_2 with a value of 2, Z_2 is the number of electrons to produce one mole of formate with a value of 8/3, and F is the Faraday constant with a value of 96,485 C mol^{-1}.

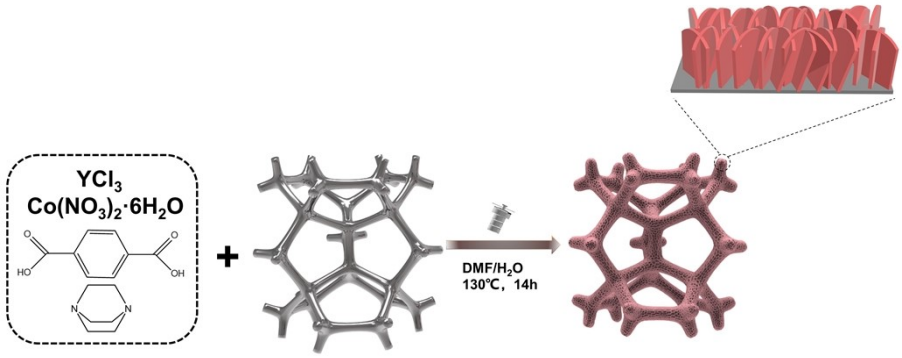

Fig. S1 Schematic diagram of the synthesis of CoY-MOF/NF.

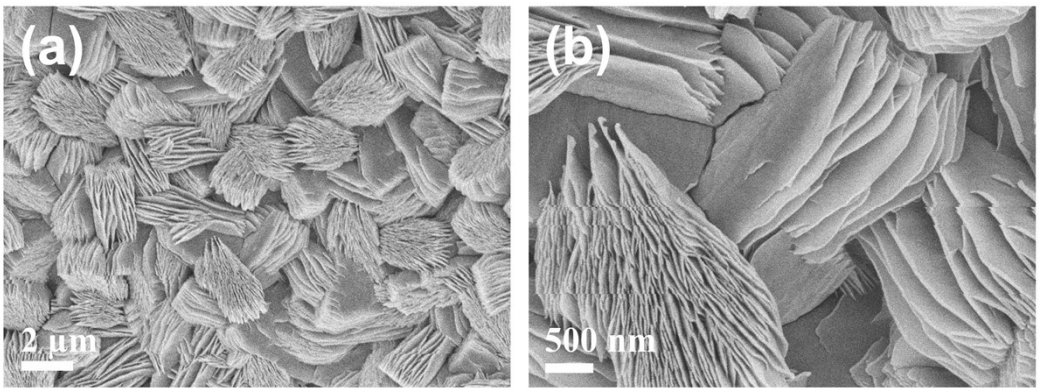

Fig. S2 SEM images of the Co-MOF/NF.

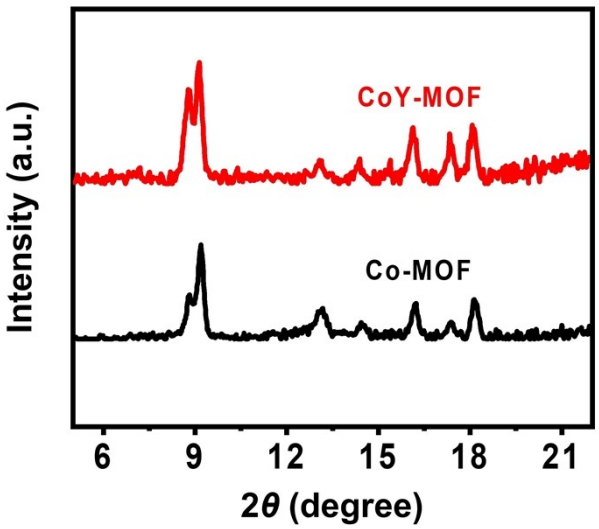

Fig. S3 XRD patterns of CoY-MOF and Co-MOF nanosheets.

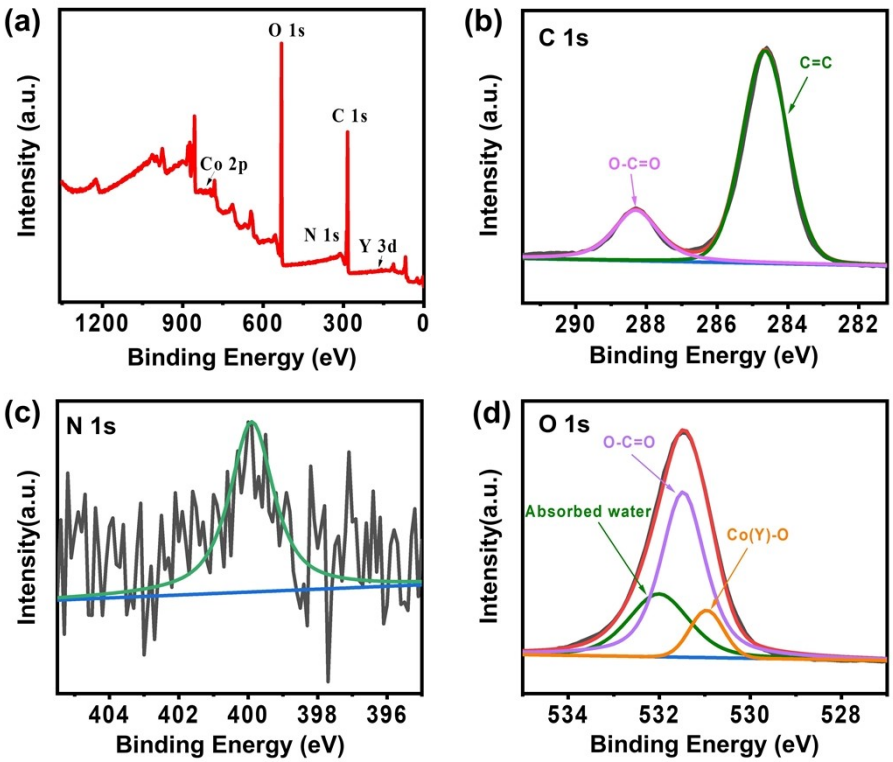

Fig. S4 (a) The XPS spectra of the CoY-MOF nanosheets. High-resolution (b) C 1s (c) N 1s, (d) O 1s XPS spectra of CoY-MOF nanosheets.

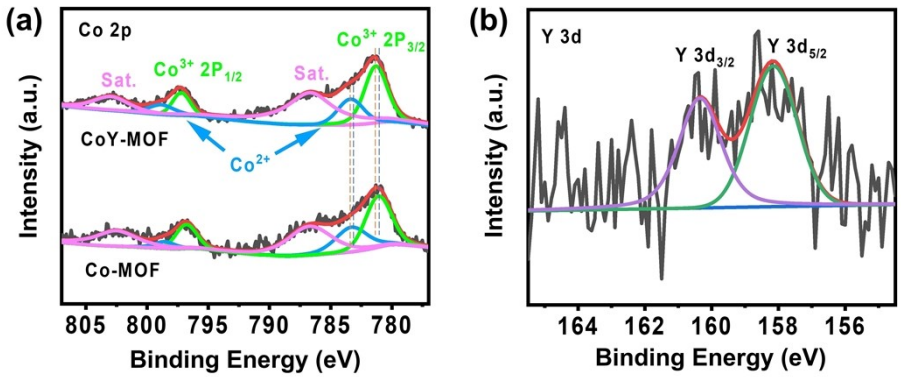

Fig. S5 (a) Co 2p high-resolution XPS spectra for CoY-MOF and Co-MOF. (b) Y 3d high-resolution XPS spectrum for CoY-MOF.

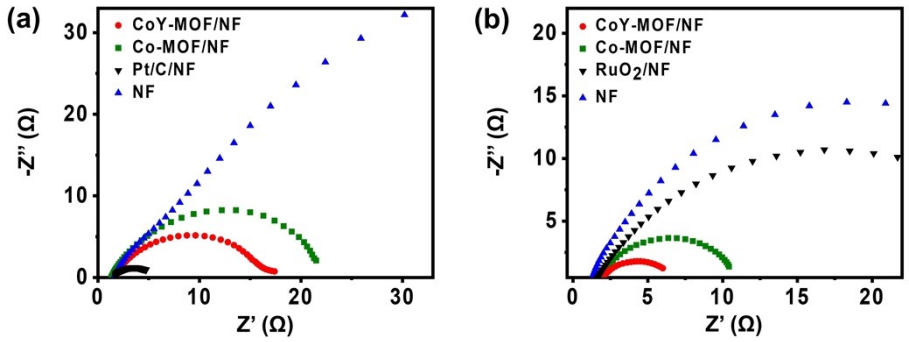

Fig. S6 Electrochemical impedance spectra of various catalysts in 1.0 M KOH without and with 0.1 M glycerol at different applied potentials: (a) -0.05 V (vs. RHE), (b) 1.4 V (vs. RHE).

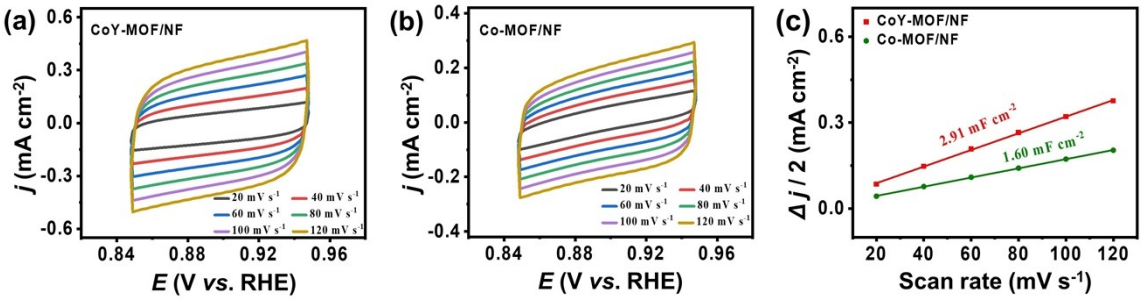

Fig. S7 Electrochemical double layer capacitance measurements of (a) CoY-MOF/NF and (b) Co-MOF/NF nanosheets at different scan rates. (c) Capacitive current density as a function of scan rate at 0.895 V (vs. RHE) for CoY-MOF/NF and Co-MOF/NF nanosheets.

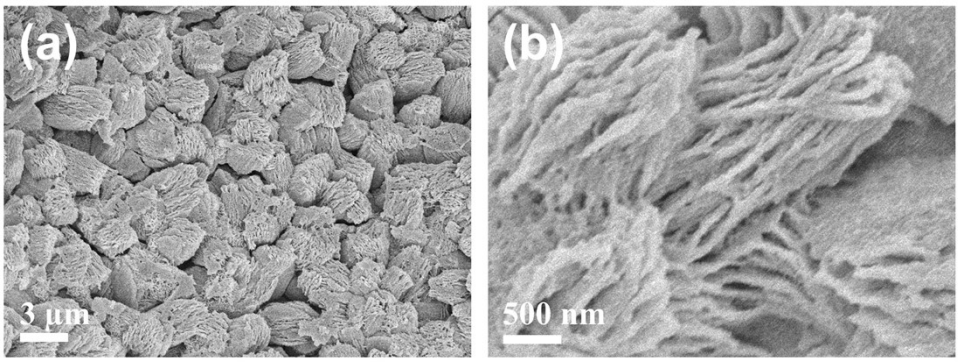

Fig. S8 SEM images of the post-HER CoY-MOF/NF.

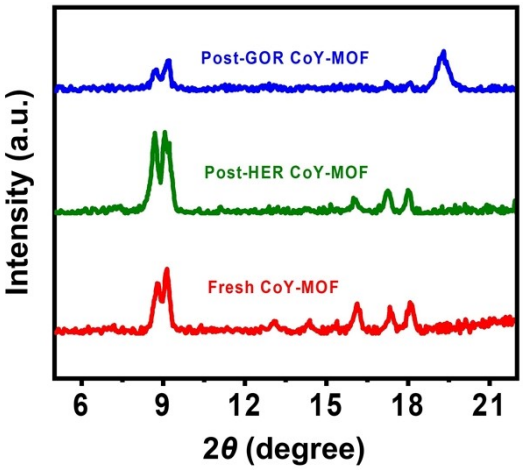

Fig. S9 XRD patterns of fresh and post-GOR, post-HER CoY-MOF nanosheets.

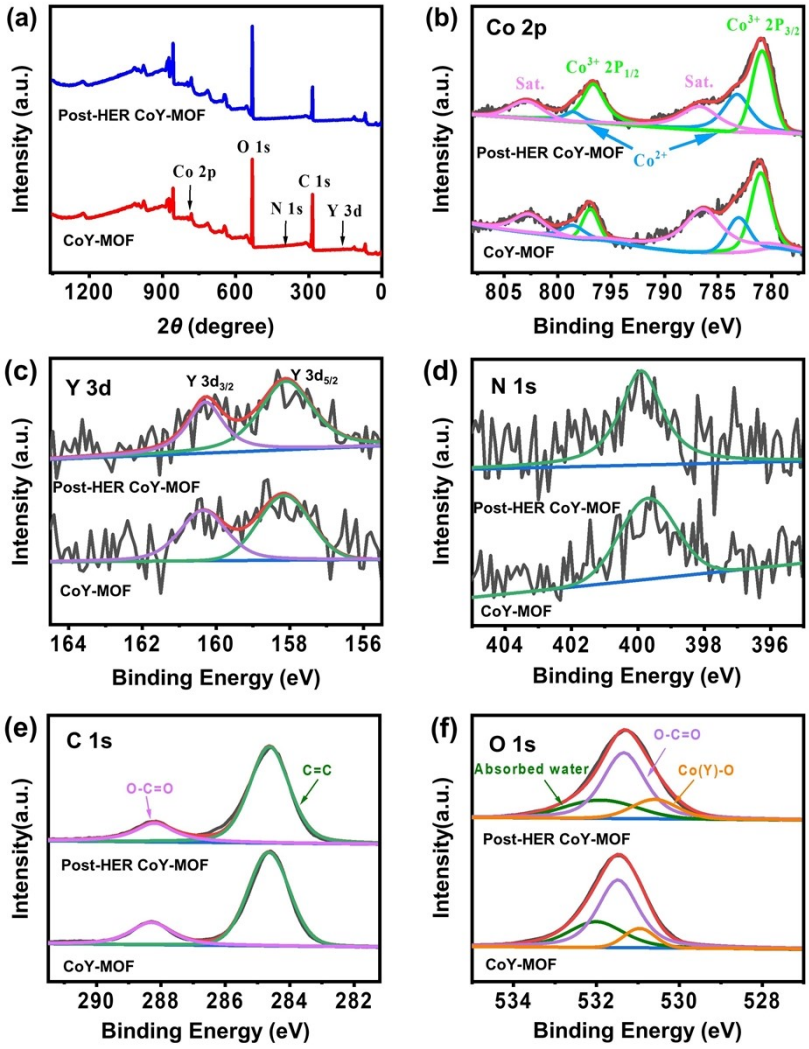

Fig. S10 (a) XPS spectra and high-resolution XPS spectra of (b) Co 2p, (c) Y 3d, (d) N 1s, and (e) C 1s (f) O 1s for the fresh and post-HER CoY-MOF nanosheets.

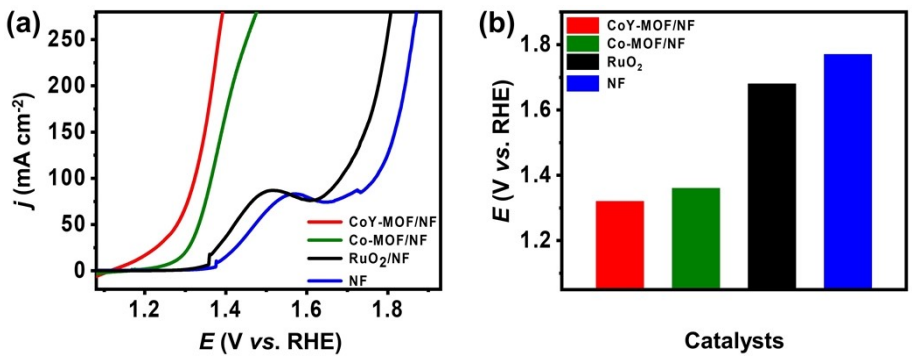

Fig. S11 (a) LSV curves of various catalysts in 1.0 M KOH with 0.1 M glycerol added. (b) Comparison of the required applied voltage at 100 mA cm^{-2} for various catalysts.

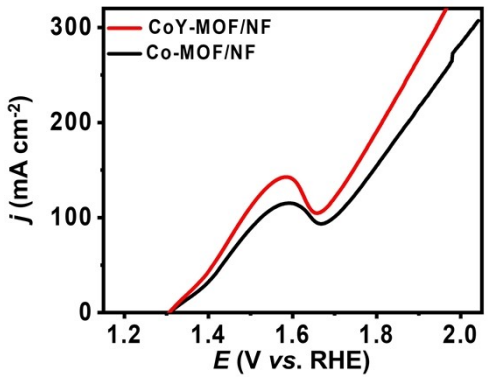

Fig. S12 LSV curves of CoY-MOF/NF and Co-MOF/NF in 1.0 M KOH solution.

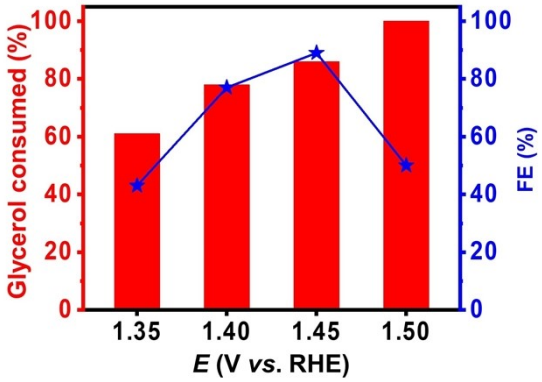

Fig. S13 FEs and glycerol consumed for formate production at varied potentials using the CoY-MOF/NF electrode.

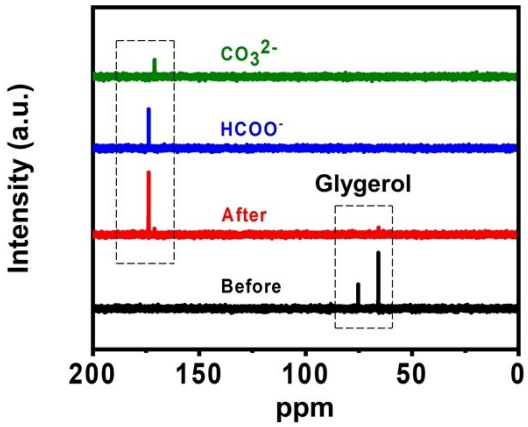

Fig. S14 ^{13}C NMR spectra of products before and after 12 h glycerol anodic oxidation on CoY-MOF/NF electrode, and the spectra of $HCOO^-$, CO_3^{2-}.

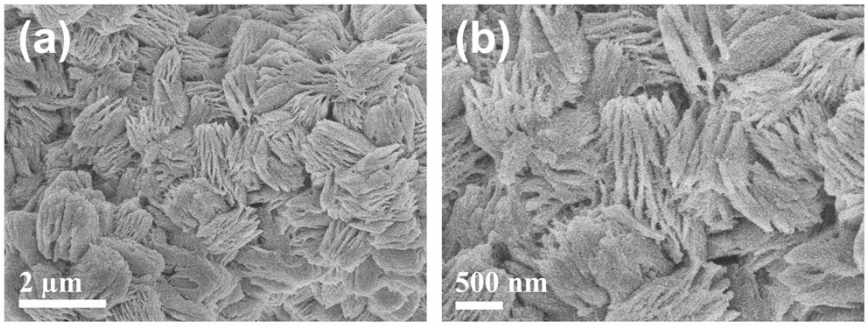

Fig. S15 SEM images of the post-GOR CoY-MOF/NF.

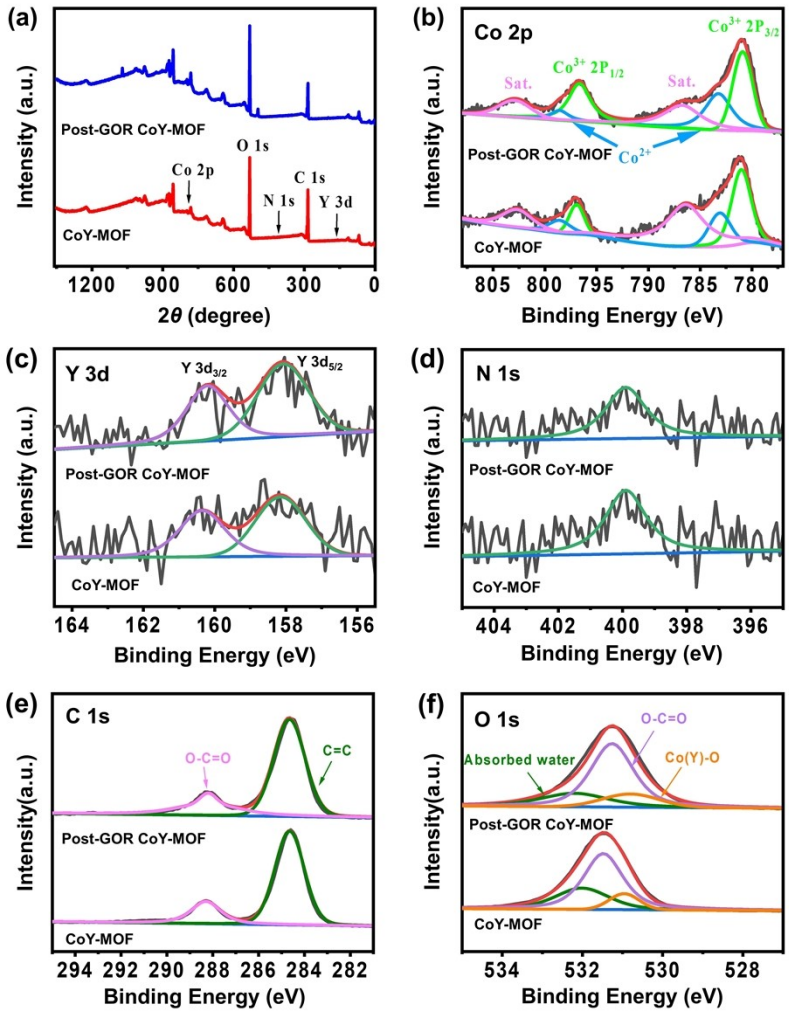

Fig. S16 (a) XPS spectra and high-resolution XPS spectra of (b) Co 2p, (c) Y 3d, (d) N 1s, and (e) C 1s (f) O 1s for the fresh and post-GOR CoY-MOF nanosheets.

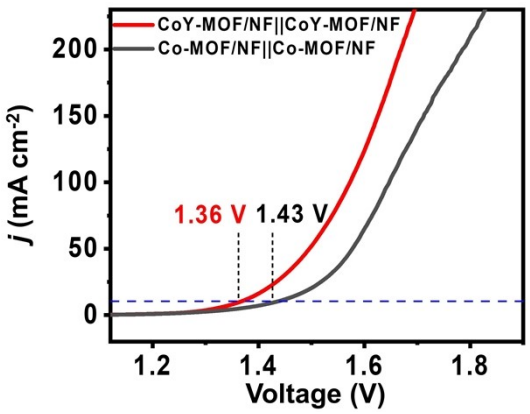

Fig. S17 LSV plots for CoY-MOF/NF||CoY-MOF /NF system and Co-MOF/NF|| Co-MOF /NF in 1.0 M KOH solution with 0.1 M glycerol.

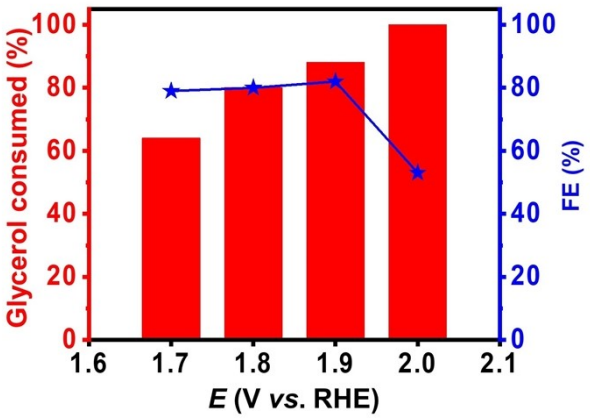

Fig. S18 FEs and glycerol consumed for formate production at varied potentials using the CoY-MOF/NF||CoY-MOF/NF two-electrode system.

Table S1. Comparison of the CoY-MOF/NF||CoY-MOF/NF system and other reported bifunctional electrocatalysts for coupling HER with other alternative anode sections.

Bifunctional catalysts	Electrolyte	Main anode product	Cell voltage (V) 10 mA cm^{-2}	Ref.
CoY-MOF/NF	**1.0 M KOH+ 0.1 M glucose**	**formate**	**1.36**	**This work**
Ni-Fe-P/NF	1 M KOH + 1.0 M ethanol	acetic acid	1.53	3
NC@$CuCo_2$Nx/CF	1 M KOH + 0.015 M benzyl alcohol	benzalzehyde	1.55	4
Ni_3S_2–Ni_3P/NF	1 M KOH + 0.5 M urea	N_2, CO_2	1.43	5
NC/Ni-Mo-N/NF	1.0 M KOH + 0.1 M glycerol	Formate	1.38	6
Co $(OH)_2$@HOS/CP	1 M KOH + 3 M methanol	formate	1.50	7
Ru&Fe-WO*x*	1 M KOH + 3 M methanol	formate	1.38	8
NiFexP@NiCo-LDH/CC	1.0 M KOH + 0.5 M methanol	formate	1.42	9
Co-S-P/CC	1 M KOH + 1.0 M ethanol	acetic acid	1.63	10
$Co_{0.83}Ni_{0.17}$/AC	1.0 M KOH + 10 mM benzyl alcohol	benzoic acid	1.43	11
Ni_2Co_1Cu LDH/NF	1.0 M KOH + 0.5 M methanol	formate	1.41	12

References

1. Y. Xu, M. Liu, M. Wang, T. Ren, K. Ren, Z. Wang, X. Li, L. Wang and H. Wang, *Appl. Catal. B: Environ.*, 2022, **300**, 120753.
2. Y. Li, X. Wei, L. Chen, J. Shi and M. He, *Nat. Commun.*, 2019, **10**, 5335.
3. S. Sheng, Y. Song, L. Sha, K. Ye, K. Zhu, Y. Gao, J. Yan, G. Wang and D. Cao, *Appl. Surf. Sci.*, 2021, **561**, 150080.
4. J. Zheng, X. Chen, X. Zhong, S. Li, T. Liu, G. Zhuang, X. Li, S. Deng, D. Mei and J.-G. Wang, *Adv. Funct. Mater.*, 2017, **27**, 1704169.
5. J. Liu, Y. Wang, Y. Liao, C. Wu, Y. Yan, H. Xie and Y. Chen, *ACS. Appl. Mater. Interfaces.*, 2021, **13**, 26948-26959.
6. Y. Xu, M. Liu, S. Wang, K. Ren, M. Wang, Z. Wang, X. Li, L. Wang and H. Wang, *Appl. Catal. B: Environ.*, 2021, **298**, 120493.
7. K. Xiang, D. Wu, X. Deng, M. Li, S. Chen, P. Hao, X. Guo, J. L. Luo and X. Z. Fu, *Adv. Funct. Mater.*, 2020, **30**, 1909610.
8. Q. Yang, C. Zhang, B. Dong, Y. Cui, F. Wang, J. Cai, P. Jin and L. Feng, *Appl. Catal. B: Environ.*, 2021, **296**, 120359.
9. Y. Zhang, X. Wu, G. Fu, F. Si, X.-Z. Fu and J.-L. Luo, *Int. J. Hydrogen. Energy.*, 2022, **47**, 17150-17160.
10. S. Sheng, K. Ye, L. Sha, K. Zhu, Y. Gao, J. Yan, G. Wang and D. Cao, *Inorg. Chem. Front.*, 2020, **7**, 4498-4506.
11. G. Liu, X. Zhang, C. Zhao, Q. Xiong, W. Gong, G. Wang, Y. Zhang, H. Zhang and H. Zhao, *New J. Chem.*, 2018, **42**, 6381-6388.
12. C. Wan, J. Jin, X. Wei, Y. Zhang, J. Wen, T. Zhu and H. Qu, *Appl. Surf. Sci.*, 2022, **598**, 153893.